Periodica Polytechnica
Chemical Engineering

61(3), pp. 227-235, 2017
https://doi.org/10.3311/PPch.9789
Creative Commons Attribution

RESEARCH ARTICLE

Simulation of Carbon Dioxide Removal by Three Amine Mixture of Diethanolamine, Methyldiethanolamine, and 2-Amino-2-Methyl-1-Propanol in a Hollow Fiber Membrane Contactor Using Computational Fluid Dynamics

Pedram Bahrami Moghim[1], Toraj Mohammadi[2*]

Received 23 July 2016; accepted after revision 14 November 2016

Abstract

The present paper investigates the simulation of carbon dioxide removal from natural gas stream by a mixture of three amines of diethanolamine (DEA), methyldiethanolamine (MDEA), and 2-amino- 2-methyl-1-propanol (AMP) in a hollow fiber membrane contactor made from polypropylene using finite volume method (FVM). The effect of structural parameters of length and thickness of membrane and diameter of shell on the removal efficiency was studied and the optimized values were calculated. The calculations were made with the assumption of two-dimensional symmetric geometry and compared with those of three-dimensional one. The effect of number and size of the meshes on the simulation results was also studied. The simulation results were validated against the experimental values from the literature. The results imply that the increase in the length and decrease in the thickness of membrane enhances the removal efficiency. As a result, higher quantities of carbon dioxide are transferred from the shell to the membrane and amine solution inside the tube which decreases the effluent CO_2 of shell and increases the average concentration of CO_2 in the membrane and tube sides. The changes in effluent CO_2 of shell with respect to amine solution concentration and influent CO_2 indicate the insignificant influence of influent CO_2 concentration on the removal efficiency.

Keywords

finite volume method, computational fluid dynamics, carbon dioxide removal, amine solution, hollow fiber membrane contactor

[1] Department of Chemical Engineering, South Tehran Branch, Islamic Azad University, Tehran, Iran

[2] Department of Chemical Engineering, School of Chemical Engineering, Iran University of Science and Technology (IUST), Narmak, 16846-13114 Tehran, Iran

* Corresponding author, e-mail: torajmohammadi@iust.ac.ir

1 Introduction

The development of industrial activities has increasingly elevated the concentration of greenhouse gases in atmosphere during the past decades. The elevation of greenhouse gases gives rise to global warming and environmental issues. Carbon dioxide (CO_2) adds up to about 80% of the aforementioned gases [1]. Conventional gas adsorption equipment such as packed, bubble and spray columns and scrubbers suffer from drawbacks like the need for large space, high capital costs and operational problems including liquid channeling, flooding, solvent loss, foaming, etc. In contrast membrane contactor technology enjoys the benefits such as, they do not suffer from operational problems; they can be operated over a wide range of flow rates and can be custom designed and modified; also, membrane contactors in form of hollow fiber offer higher surface area 1600-6500 m^2/m^3 as compared with conventional tray towers or packed columns with 30-330 m^2/m^3. Besides, less energy consumption, easy scale up, and independent control of gas and liquid rates are other traits than can characterize them as a capable technology [1,2]. CO_2 removal by membrane contactors has been studied since 1980's and the researchers have investigated factors such as solvent type, membrane material, and modulus type etc. to improve its performance. The membrane contactor technology benefits from both separation processes of membrane and adsorption. Qi and Cussler [3, 4] first implemented the idea of hollow fiber membrane contactor (HFMC) application for the adsorption of CO_2 using non-wetted polypropylene membrane with porosity of several micrometres and aqueous sodium hydroxide as the adsorbent. Separation of CO_2 by membrane contactors provides more than 70% and 66% reductions in size and weight and up to 10 times adsorption capacity, respectively, compared to the conventional methods [5]. Gas phase flows in one side of HFMC (tube or shell side) and the liquid adsorbent phase flows in the other side while the two streams are not dispersed within each other. In case of hydrophobic membranes (e.g. polypropylene membranes) the gas-liquid interface forms inside the porous volume in the vicinity of the liquid phase (non-wetted operation) [2] and the gas diffuses in the membrane mostly because of concentration

gradient and less likely as a result of pressure gradient, however it depends on the applied pressure and flow velocity [6]. Zhang et al. [7] studied the chemical adsorption of CO_2 by aqueous diethanolamine (DEA) in HFMC and realized that CO_2 flux is significantly influenced by influent gas velocity and merely by influent liquid velocity. The limiting factor for the reaction rate of CO_2 and DEA was the CO_2 concentration in the gas phase. They found an effective length of membrane modules wherein the removal efficiency reached a maximum value. Sohrabi et al. [8] studied the chemical adsorption of CO_2 in HFMC by finite elements method and observed the highest CO_2 removal using monoethanolamine (MEA). The highest CO_2 removal was obtained by first, 2-amino- 2-methyl-1-propanol (AMP) and second, DEA in a research conducted by Saidi et al. [9] on the effect of DEA, methyldiethanolamine (MDEA), AMP, and mixture of DEA and MDEA on CO_2 removal. Their findings imply the improvement of removal efficiency by an increase in liquid velocity, number of fibers, temperature and decrease in gas velocity. Wang et al. [10] utilized three alkanolamine solutions of AMP, DEA, and MDEA as the adsorbent for their simulation of CO_2 adsorption in HFMC. The results indicated the higher capability of AMP and DEA for the adsorption of CO_2 when compared to MDEA. However, their concentrations in the solution dropped dramatically. Accordingly, a solution of amines like DEA, MDEA and AMP has been chosen due to better performance in removal of CO_2 from the standpoint of reactivity, absorption capacity (different CO_2 loading factor of absorbents), regeneration performance, higher selectivity and synergetic effects [8, 10, 11].

2 Model development

Hollow fiber membrane contactor comprises three sections: shell, membrane, and tube. The amine solution (liquid phase) flows in the tube side while the natural gas containing CO_2 flows in the shell side in the opposite direction. The CO_2 removal process includes three steps: the diffusion of gas component from the gas bulk to the external surface of the membrane, the diffusion in the membrane pores, dissolution in the solvent (adsorbent) and chemical reaction. The schematic diagram of the membrane modulus and its physical specifications are presented in Fig. 1 and Table 1 respectively. The following assumptions were made for the mathematical modelling of the membrane:

1. The diffusion of other components of natural gas in the membrane is excluded.
2. CO_2 concentration variations and its partial pressure in the tube side are assumed to be negligible.
3. Isothermal condition is prevailed throughout the modulus.
4. The fluids flow is fully developed and laminar (Reynolds number less than 100).
5. The membrane is assumed to be impermeable to the amine solution which is mostly correct for polypropylene membranes
6. At the initial conditions, the shell and tube sides are supposed to be full of gas and amine solution, respectively. Therefore, there are effluents from both sides since the beginning of the simulation process.
7. The gas phase is assumed to be an ideal gas.
8. The Henry's law governs the gas-liquid equilibrium.

Table 1 Specifications of membrane modulus used for modeling

Parameter	Value
Shell length (mm)	400-200-100
Shell diameter (mm)	12-10-8
Membrane thickness (mm)	0.6-0.4-0.2-0.1
Membrane length (mm)	400-200-100
Porosity	0.6
Tortuosity	3.5

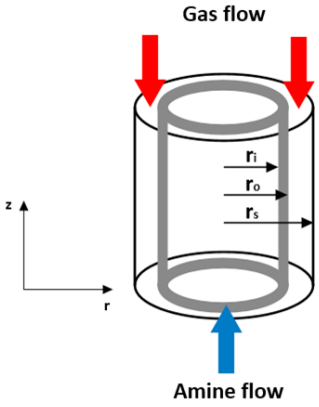

Fig. 1 Shematic Diagram of Holow Fiber Membrane Contactor

The total continuity (mass conservation), motion (momentum conservation), and CO_2 partial continuity equations are presented in equations of (1), (2), and (3) respectively:

$$\frac{\partial \rho}{\partial t} + \nabla \cdot (\rho \mathbf{u}) = 0 \tag{1}$$

$$\rho \frac{\partial \mathbf{u}}{\partial t} + \rho (\mathbf{u} \cdot \nabla)\mathbf{u} = \nabla \cdot [-p\mathbf{I} + \tau] + \mathbf{F} \tag{2}$$

$$\frac{\partial c_{CO_2}}{\partial t} + \nabla \cdot \left(-D_{CO_2} \nabla c_{CO_2}\right) + \mathbf{u}_{co_2,g} \cdot \nabla c_{CO_2} = R_{CO_2} \tag{3}$$

Where $\boldsymbol{\rho}$ is the fluid density (kg/m^3), $\mathbf{u}$ is the velocity vector (m/s), $\mathbf{p}$ is the pressure (Pa), $\mathbf{I}$ is the identity matrix, $\boldsymbol{\mu}$ is the dynamic viscosity (kg/(m.s)), $\mathbf{F}$ is the body force (N/m^3) which is equal to zero in the present system, $\mathbf{c_{CO2}}$ is the CO_2 concentration (mol/m^3), $\mathbf{D_{CO2}}$ is the diffusivity of CO_2 (m^2/s), and $\mathbf{R_i}$ is the rate of reaction with amine (mol/m^3.s).

2.1 Tube Side

Carbon dioxide partial continuity equation (3) in the tube side at steady state conditions takes the form of Eq. (4):

$$D_{co_2,l}\left(\frac{\partial^2 c_{co_2,l}}{\partial r^2}+\frac{1}{r}\frac{\partial c_{co_2,l}}{\partial r}+\frac{\partial^2 c_{co_2,l}}{\partial z^2}\right)=u_l\frac{\partial c_{co_2,l}}{\partial z}-\mathrm{R}_{CO_2} \tag{4}$$

Where $D_{CO2,l}$ is the diffusivity of CO_2 in the liquid (amine solution) phase, $c_{CO2,l}$ is the concentration of CO_2 in the liquid phase, and u_l is the liquid axial velocity profile which can be calculated from Eq. (5) for laminar flow in hollow fibers [12]:

$$u_l=2\bar{u}_l\left(1-\left(\frac{r}{r_i}\right)^2\right) \tag{5}$$

Where $\bar{u}_l$ is the liquid average velocity, r is the radial distance from the central axis, and r_i is the fiber internal radius. The boundary conditions for the solution of Eq. (4) are shown in Eqs. (6) to (9) under the assumptions of symmetry along the fiber radius and the non-volatility of the adsorbent:

$$z=0,\quad \mathrm{c}_{co_2,l}=0,\quad c_{a\min e,i}=c_{a\min e,i0} \tag{6}$$

$$z=L,\quad \mathrm{N}_{co_2}=\mathrm{c}_{co_2}u_l \tag{7}$$

$$r=0,\qquad \frac{\partial \mathrm{c}_{co_2,l}}{\partial r}=0,\qquad \frac{\partial \mathrm{c}_{\mathrm{amine,i}}}{\partial r}=0 \tag{8}$$

$$r=r_i,\qquad \mathrm{c}_{co_2,l}=Hc_{co_2,m},\qquad \frac{\partial \mathrm{c}_{a\min,i}}{\partial r}=0 \tag{9}$$

Where $c_{Amine,I}$ is the concentration of amine type I, $c_{CO2,m}$ is the CO_2 concentration at the membrane-liquid interface, N_{CO2} is the CO_2 advective molar flux (mol/m^2.s), and H is the Henry's law constant. Henry's law was used to describe the equilibrium concentration of solute at the membrane-liquid interface and liquid phase given the fact that the CO_2 concentration is very low in the liquid phase and it's consumed quickly in the chemical reaction. The initial concentrations of each amine type were set to 0.5 mol/m^3. The diffusivity of CO_2 in amine solution may be predicted by Eq. (10) [13]:

$$D_l=2.35\times10^{-6}\exp\left(-\frac{2119}{T}\right) \tag{10}$$

Where T is the absolute temperature and equal to 298 K.

2.2 Shell Side

The gas flow velocity distribution in the shell side is obtained by solving total continuity and motion (Navier-Stokes) equations (Eqs. (1) and (2)). The gas flow in the shell side is assumed to be isothermal, isobaric, and incompressible. The no-slip condition (u=0 m/s) applies to both interior and exterior walls. The inflow and outflow streams are described as Eqs. (11), (12), and (13) respectively.

$$\mathbf{u}_{CO_2}=-u_{inlet,CO_2}\mathbf{n} \tag{11}$$

$$\left[-p\mathbf{I}+\mu_{co_2}\left(\nabla\mathbf{u}_{co_2}+\left(\nabla\mathbf{u}_{co_2}\right)^T\right)-\frac{2}{3}\mu_{co_2}\left(\nabla.\mathbf{u}_{co_2}\right)\mathbf{I}\right]\mathbf{n}=-\hat{p}_0\mathbf{n} \tag{12}$$

$$\hat{p}_0\le p_0 \tag{13}$$

Where $\mathbf{u_{inlet,CO2}}$ is the scalar value of influent CO_2 (m/s) and $\mathbf{p_0}$ is equal to relative zero (atmosphere). The initial values are as Eqs. (14) and (15):

$$\mathbf{u}_{0,co_2}=0\,m/s \tag{14}$$

$$\boldsymbol{P}_{0co2}=0\,pa \tag{15}$$

Continuity equation for CO_2 (Eq. (3)) in the shell side is expressed as Eq. (16):

$$u_g\frac{\partial c_{co_2,g}}{\partial z}=D_{co_2,g}\left(\frac{\partial^2 c_{co_2,g}}{\partial r^2}+\frac{1}{r}\frac{\partial c_{co_2,g}}{\partial r}+\frac{\partial^2 c_{co_2,g}}{\partial z^2}\right) \tag{16}$$

Where $\mathbf{D_{CO2,g}}$ and $\mathbf{c_{CO2,g}}$ are the diffusivity and concentration of CO_2 in the gas phase respectively. $\mathbf{D_{CO2,g}}$ is combined of intramolecular interactions (self-diffusion) and molecular interactions with the pore wall (Knudsen diffusion) and found to be 2.2×10^{-6} m/s in the present system. The boundary conditions are as follows (Eqs. (17) to (20)):

$$r=r_0\qquad \mathrm{Z}=\mathrm{z}\qquad \mathrm{c}_{co_2,\mathrm{g}}=\mathrm{c}_{co_2,\mathrm{m}} \tag{17}$$

$$r=r_e\qquad \mathrm{Z}=\mathrm{z}\qquad \frac{\partial c_{co_2,g}}{\partial r}=0 \tag{18}$$

$$z=0\qquad \mathrm{N}_{co_2,\mathrm{g}}=\mathrm{c}_{co_2}\cdot u_g \tag{19}$$

$$z=L\qquad \mathrm{c}_{co_2}=\mathrm{c}_0 \tag{20}$$

In which $\mathbf{r_0}$ is the outer membrane radius, $\mathbf{c_0}$ is the CO_2 concentration in the influent gas, $\mathbf{N_{CO2}}$ is the advective mass transfer flux, and $\mathbf{r}_e$ is the shell effective radius which may be calculated from Eq. (21) using Happel's free surface model [14]:

$$r_e=\left(\frac{1}{1-\varphi}\right)^{0.5}r_0 \tag{21}$$

Where φ is the fibers void fraction.

2.3 Membrane Side

Since mass transfer is governed by molecular diffusion within the membrane, the continuity equation for CO_2 is expressed as Eq. (22) in this region:

$$D_{co_2,m}\left(\frac{\partial^2 c_{co_2,m}}{\partial r^2}+\frac{1}{r}\frac{\partial c_{co_2,m}}{\partial r}+\frac{\partial^2 c_{co_2,m}}{\partial z^2}\right)=0 \tag{22}$$

D_{CO2} is the diffusivity of CO_2 in the membrane. The boundary conditions are as Eqs. (23) and (24):

$$r = r_i \qquad c_{co_2,m} = \frac{c_{co_2,l}}{H} \tag{23}$$

$$r = r_0 \qquad c_{co_2,m} = c_{co_2,g} \tag{24}$$

The value of $\mathbf{D_{CO2,m}}$ may be obtained from Eq. (25):

$$D_{CO_2,m} = D_{CO_2,g}\left(\frac{\varepsilon}{\tau}\right) \tag{25}$$

Where ε and τ represent porosity and tortuosity respectively.

3 Mass Transfer Mechanism

The resistances-in-series model may be used to express the gas adsorption in hollow fibers by liquid (Fig. 2). The total resistance is the sum of the resistances of gas, membrane, and liquid phases.

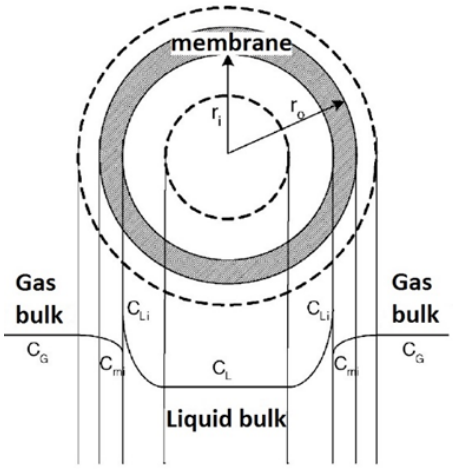

Fig. 2 Mass transfer process in gas-liquid hollow fiber membrane contactor

Overall mass transfer coefficient in the liquid phase (K_{OL}) is expressed as Eq. (26):

$$\frac{1}{K_{OL}} = \frac{m}{k_g d_o/d_l} + \frac{m}{k_m d_{lm}/d_l} + \frac{1}{k_l} \tag{26}$$

Where $\mathbf{k_g}$, $\mathbf{k_m}$, and $\mathbf{k_l}$ are the local mass transfer coefficients in gas, membrane, and liquid phases respectively; d_o, d_i, and d_{lm} are the outer, inner, and logarithmic average diameters of hollow fibers respectively; m is the distribution factor between gas and liquid phases; and E is the enhancement factor resulting from chemical reaction. The membrane resistance depends on the operation type i.e. wetting, non-wetting, and partial wetting modes. The membrane resistance for pores fully filled by gas or liquid is a function of the diffusivity of CO_2 in the gas phase ($\mathbf{D_{CO2,g}}$) or liquid phase ($\mathbf{D_{CO2,l}}$) and the geometric characteristics such as thickness (**δ**), porosity (**ε**), and tortuosity (**τ**) of the membrane [4]. Non-wetting operation is the best mode for membrane contactors because their resistance approaches the minimum in these conditions. Pressure balance of gas-liquid operation, utilizing more hydrophobic membranes, using liquid adsorbents of higher surface tensions, and membrane structure with smaller pores improve the non-wettability of the separation process. It is better to adopt a liquid flow in the tube side and a gas flow in the sell side for gas adsorption processes. The liquid mass transfer coefficient ($\mathbf{k_l}$) can be calculated by Graetz-Leveque correlation (Eq. (27)) [2]:

$$Sh = \frac{k_l d_i}{D_{CO_2,l}} = 1.62\left(\frac{d_i}{L}\mathrm{Re}\cdot Sc\right)^{\frac{1}{3}} \tag{27}$$

Sh is Sherwood number, **Re** is Reynolds number, and **Sc** is Schmidt number. The CO_2 mass transfer coefficient in the gas phase can be calculated by Yang and Cussler correlation (Eq. (28)) [15]:

$$Sh = \frac{k_g d_e}{D_{CO_2,g}} = 1.25\left(\frac{d_e}{L}\mathrm{Re}\right)^{0.93} Sc^{0.33} \tag{28}$$

Where $\mathbf{d_e}$ is the shell hydraulic diameter. Mass transfer coefficient of CO_2 in the membrane ($\mathbf{k_{CO2,g,m}}$) is expressed as Eq. (29):

$$k_{CO_2,g,m} = \frac{D_{CO_2,g}\varepsilon}{\tau\delta} \tag{29}$$

3.1 Mass Transfer Mechanism

The blend of three amines of AMP (type I amine), DEA (type II amine), and MDEA (type III amine) were studied in the present study. Their chemical structure and physical properties are shown in Fig. 3 and Table 2 respectively [10].

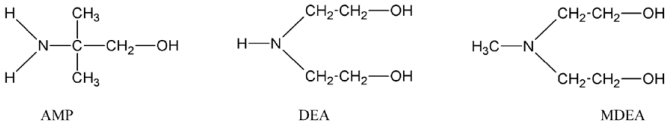

Fig. 3 Chemical structure of AMP, DEA, and MDEA [10]

Table 2 Physical properties of the three amines at the room temperature [10]

Aqueous amine solution	$D_A \times 10^9$ (m^2s^{-1})	$D_B \times 10^9$ (m^2s^{-1})	Concentration ($kmolm^{-3}$)
AMP	1.33	9.7	0.5
DEA	1.25	5.95	0.5
MDEA	1.25	9.74	0.5

The reaction of type I or II amines (R_1R_2NH) with dissolved CO_2 is described by the two-step zwitterion mechanism. In the first step, the intermediate zwitterion is formed (30):

$$CO_2 + R_1R_2NH \underset{k_{-1}}{\overset{k_2}{\rightleftharpoons}} R_1R_2NH^+CO_2^- \tag{30}$$

Then, the zwitterion is deprotonated by the available bases in the solution and forms **a** carbamate ion and a protonated base (Eq. (31)) [16]:

$$R_1R_2NH^+CO_2^- + b \underset{}{\overset{k_b}{\rightleftharpoons}} R_1R_2NCO_2^- + bH^+ \quad (31)$$

Where **b** represents H_2O, OH^- and R_1R_2NH in the amine solution, respectively. Based on the assumption of quasi steady state condition for the zwitterions concentration, the rate of CO_2 reaction with type I or II amines is described by Eq. (32) [10]:

$$R_{CO_2} = \frac{k_2[CO_2][R_1R_2NH]}{1+\left(k_{-1}/k_{H_2O}[H_2O]\right)+\left(k_{-1}/k_{OH^-}[OH^-]\right)+\left(k_{-1}/k_{R_1R_2NH}[R_1R_2NH]\right)} \quad (32)$$

The contribution of OH^- is negligible compared to those of H_2O and R_1R_2NH. The kinetic parameters for amine solutions of AMP, DEA, and MDEA are listed in Table 3.

Table 3 Kinetic parameters of three types of amine at the room temperature

Aqueous amine solution	k_2 ($m^3kmol^{-1}s^{-1}$)	$k_2 k_{R_1R_2NH}/k_{-1}$ ($m^6kmol^{-2}s^{-1}$)	$k_2 k_{H_2O}/k_{-1}$ ($m^6kmol^{-2}s^{-1}$)
AMP	810	2335	2.64
DEA	2375	437	2.2
MDEA	2.47	-	-

Type III amine doesn't undergo the reactions (30) and (31) because there is not any hydrogen bond with nitrogen. The reaction of Type III amine with CO_2 is advanced by the formation of a protonated amine and a bicarbonate anion (Eq. (33)) [16]:

$$R_1R_2R_3N + H_2O + CO_2 \xrightarrow{k_2} R_1R_2R_3NH^+ + HCO_3^- \quad (33)$$

The overall rate of reaction between CO_2 and MDEA solution is second degree (Eq. (34)):

$$R_{CO_2} = K_2[MDEA][CO_2] \quad (32)$$

The rate constant correlates to temperature via Arrhenius equation (Eq. (35)):

$$k_2 = 8.741\times10^{12}\exp\left(-\frac{8625}{T}\right) \quad (35)$$

3.2 Solution of Equations

The total and partial continuity and motion equations were solved by finite volume method using COMSOL Multiphysics 5 software. The discretization of equations was made using variable size triangular meshes. The solution at steady state and transient state was made by GMRES and MUMPS solvers respectively. The calculations iterations and tolerance were adjusted to 10 and 10^{-4} respectively. The time interval was chosen as 30 seconds in the transient state. The solution of equations necessary for the simulation of adsorption process in membrane contactors by means of finite elements method using COMSOL software was also studied by Gilassi et al. [17] (triangular mesh, PARDISO solver) and Razavi et al. [11] (triangular mesh, UMFPACK solver).

4 Results and Discussion

The influent gas and amine solution velocities were adjusted to 0.0157 and 0.27 m/s respectively. The increase in influent gas velocity decreases the gas holdup time and the removal rate of CO_2, however, the increase in adsorbent (amine) liquid velocity elevates the turbulence of boundary layer which prevents the adsorbent from being saturated by CO_2. The influent CO_2 concentration in gas and liquid phases were chosen as 100 and 0 ppm respectively. The three dimensional geometry of the membrane was approximated to a two dimensional one to reduce the calculations. Mesh number was set to 288750 and 14830 in three and two dimensional modes, respectively. The results of two and three dimensional geometries as the diagrams of average CO_2 concentrations in the shell, membrane, and tube sides are depicted in Fig. 4. They indicate a small difference between the two geometries results. Considering an 88% reduction in the calculations time (from 1340 to 158 minutes), the advantage of applying the two dimensional approximation is clear.

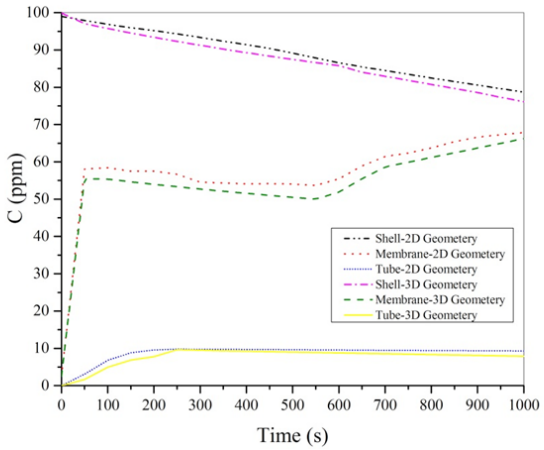

Fig. 4 Comparison of CO_2 concentration variations in shell, tube, and membrane sides between two and three dimensional geometries

4.1 The Effectof Size and Number of Meshes

Table 4 shows the effect of mesh number on the effluent CO_2 concentration from the shell side. The velocity, temperature, and Reynolds number of the influent gas to the shell side were 0.27 m/s, 273 K, and 80. The velocity, temperature, and Reynolds number of the influent amine solution to the tube side were 0.0157 m/s, 273 K, and 100. Although the increase in mesh number improves the precision of calculations, it also increases the calculations time and iterations. It also increases the cumulative error resulting in the decrease of the precision. Therefore, an optimum value for the mesh number should be chosen.

Table 4 The effect of mesh number on the simulation results (length=200 mm)

Mesh number	Average velocity of the shell effluent(m/s) *	Average CO_2 concentration of the shell effluent (ppm) *
25457	0.195	62.429
61070	0.216	64
98976	0.218	64.02
238078	0.219	64.03

* After 17 minutes

The mesh size was smaller in the regions where the CO_2 concentration variations were higher and vice versa. As seen in table 4, the increase of mesh number from 61070 to 98976 and higher didn't cause any significant change in the simulation results. Therefore, the calculations precision was independent of the mesh number for values greater than 61070.

4.2 The Effect of Membrane and Shell Length

The effect of membrane length on the removal efficiency was studied at the membrane thickness of 2 mm, shell diameter of 10 mm, and influent CO_2 concentration of 100 ppm. The results are depicted in Fig. 5. The increase in the membrane length slightly decreases the effluent CO_2 concentration and increases the removal efficiency. The same trend is reported by Farjami et al. [18]. The increase in length decreases the average CO_2 concentration in the membrane. For example, the average CO_2 concentration reaches 69 ppm at the length of 100 mm and 65 ppm at the length of 400 mm after 1000 seconds. Hence, the biggest value i.e. 400 mm was chosen as the desired value for the membrane length.

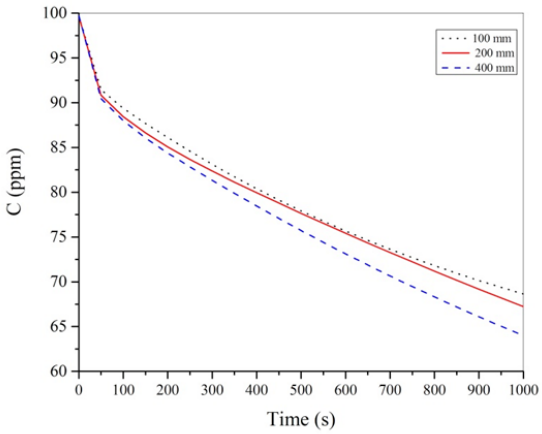

Fig. 5 CO_2 concentration in effluent gas of shell side with time at different membrane lengths

The increase in the membrane length raises its separation surface so that the effluent CO_2 concentration falls. As a result, the concentration gradient between the two sides and the membrane CO_2 concentration decrease (Fig. 6)

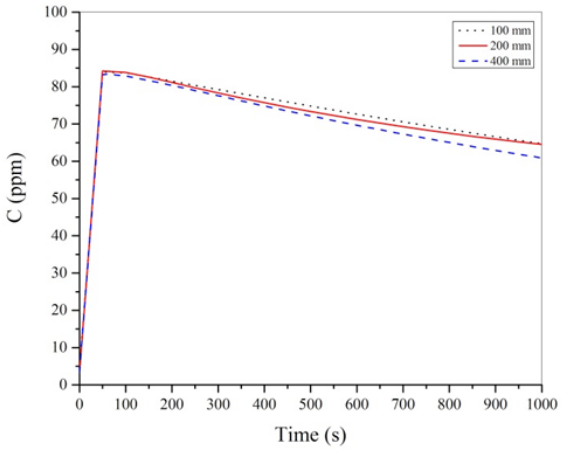

Fig. 6 CO_2 concentration in the membrane with time at different membrane lengths

CO_2 concentration in the effluent amine solution increases with the increase in the membrane length (Fig. 7). As mentioned earlier, the increase in membrane length enhances the removal efficiency and concentration gradient with time which ultimately increases the effluent CO_2 concentration in the amine solution.

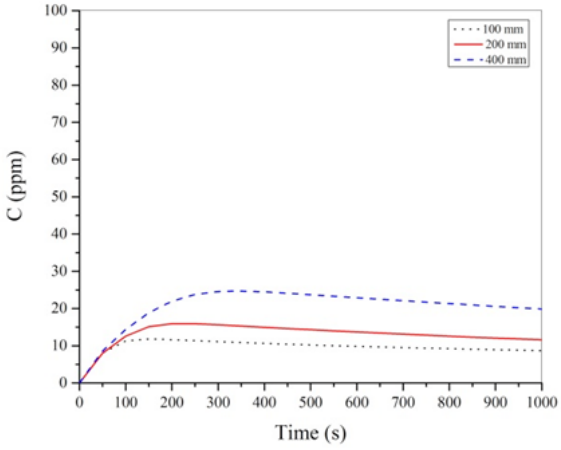

Fig. 7 CO_2 concentration in the effluent amine solution of tube side with time at different membrane lengths

4.3 The Effect of Membrane Thickness

The effect of membrane thickness on the CO_2 concentration in the different sections of membrane contactor is tabulated in Table 5. As the thickness increases, the resistance to mass transfer increases so that the average CO_2 concentration in the effluent from the shell side increases and the average concentration of CO_2 in the membrane and tube decreases. For example, as the thickness increases from 0.1 to 0.4 mm, the average CO_2 concentration in the tube effluent and the membrane decreases by 2.10 and 2.29 ppm respectively. At the same time, the average CO_2 concentration in the effluent from the shell side increases by 4.53 ppm. The minimum membrane thickness i.e. 0.1 mm is the optimum value.

Table 5 The effect of membrane thickness on CO_2 concentration at different sections of the modulus

Thickness (mm)	Average CO_2 concentration in shell effluent (ppm)	Average CO_2 concentration in membrane (ppm)	Average CO_2 concentration in tube effluent (ppm)
0.1	46.35	62.21	22.44
0.2	47.64	60.88	21.25
0.4	50.88	59.92	20.54
0.6	52.45	58.18	20.48

4.4 The Effect of Shell Diameter

The effect of shell diameter on the effluent CO_2 concentration was investigated at the membrane thickness of 2 mm, length of 200 mm, and influent CO_2 concentration of 100 ppm. The increase in shell diameter results in the elevation of gas volume in the shell side which reduces the rate of CO_2 concentration decrease with time. The increase in shell volume causes increase in the CO_2 concentration in the shell side which provides higher concentration gradient and driving force for mass transfer. It results in higher removal efficiencies. However, elevated amounts of CO_2 enter the shell side so that the increase in the shell diameter increases the effluent CO_2 concentration.

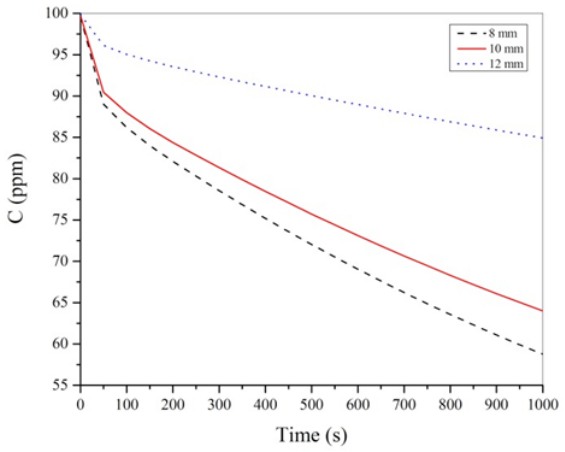

Fig. 8 The CO_2 concentration in the effluent from shell side at different shell diameters

Alcora - Castell&oacutebetween the tube and shell sides (Fig. 9).

The high accumulation of CO_2 concentration in the membrane pores reduces the CO_2 entering the amine solution, therefore less amounts of CO_2 enter the amine solution. Hence, the effluent CO_2 concentration from the tube side is reduced.

The optimum parameter values and the CO_2 concentrations at different sides are represented in Table 6 and Fig. 11 respectively.

Table 6 Optimum membrane parameters

Membrane length	Shell diameter	Membrane thickness	Meshing
400 mm	8 mm	0.1 mm	61070

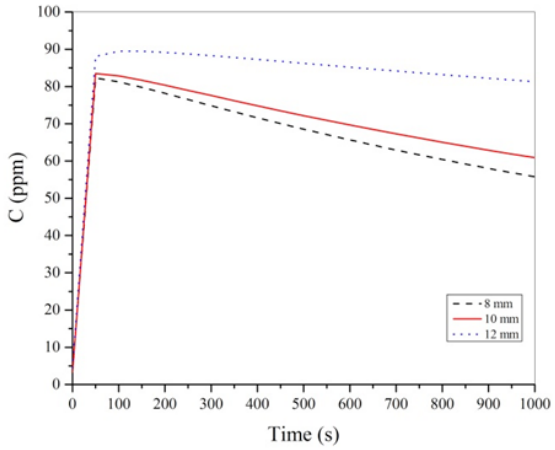

Fig. 9 The average CO_2 concentration in the membrane at different shell diameters

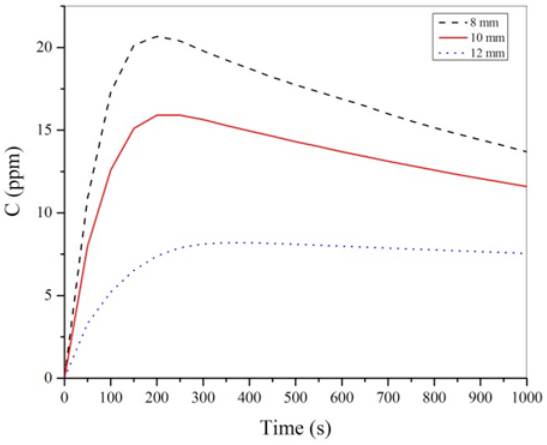

Fig. 10 The average CO_2 concentration in the effluent from tube side at different shell diameters

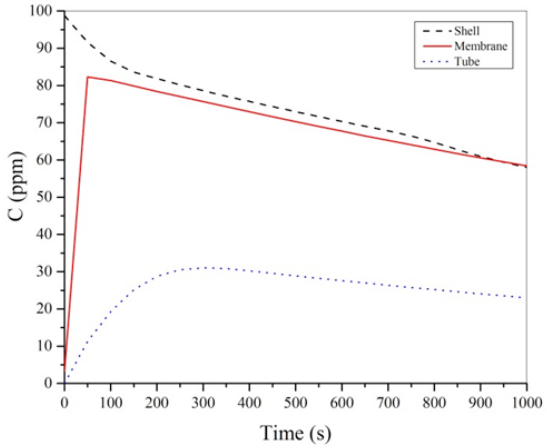

Fig. 11 CO_2 concentration in different membrane contactor sections at the optimum conditions

5 Validation

The validation of the simulation results of the present study was carried out by comparing the results with those obtained by Wans et al. [10]. They used AMP, DEA, and MDEA aqueous solutions separately at initial concentrations of 1.56, 1.2, and 1.2 mol/m^3 respectively. The mixture of all three amines with the initial concentration of 1.5 mol/m^3 was used in the present study. The relative concentrations of CO_2 with respect to radius are illustrated in Fig. 12. It can be seen that CO_2 concentration is maximum at the furthest point of the shell side but it decreases as the distance from the membrane surface decreases. As CO_2 enters the amine solution flowing in the tube side, it's quickly consumed because of the high reaction rate. The falling trend is smoother for MDEA compared to AMP and DEA. The blend of all three amines showed a trend which is an average of the three single amines.

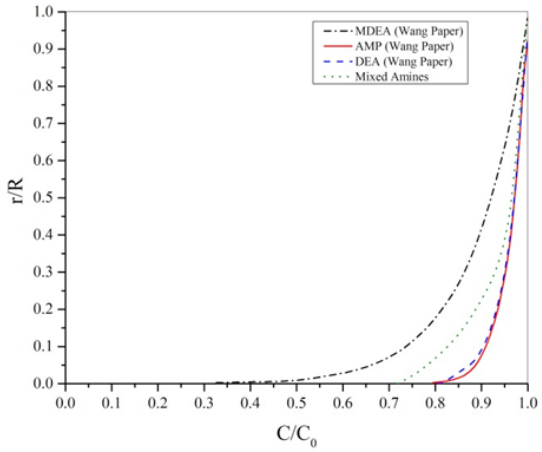

Fig. 12 Relative CO_2 concentration at different distances

6 Conclusion

The CO_2 removal by a mixture of three amine types in a hollow fiber membrane contactor was studied in the present study. Mathematical modelling was performed based on the continuity and momentum equations taking into account the advective and diffusive mass transfer in the shell and tube sides, molecular diffusion in the membrane, and chemical reaction in the tube side. Partial differential equations system was solved by finite volume method using COMSOL software. The concentration profile was determined in different sections of the membrane modulus and the validation of model was confirmed through comparison with the experimental values in the literature. The effect of membrane and shell length, membrane thickness, and shell diameter on the removal efficiency was studied. The increase in membrane length results in the increase in removal efficiency. The decrease in the membrane thickness causes decrease in the resistance to the mass transfer leading to introduction of higher CO_2 amounts from the gas phase in the shell side to the solution flowing in the tube side. The increase in the shell diameter causes less amounts of CO_2 entering the amine solution because of higher accumulation of CO_2 concentrations in the membrane pores. The influent CO_2 concentration has a negligible effect on the removal process because it reacts fast with the amine solution. The CO_2 concentration changes in the effluent form the shell side have a linear functionality with respect to the influent CO_2 concentration.

References

[1] Al-Marzouqi, M. H., El-Naas, M. H., Marzouk, S. A. M., Al-Zarooni, M. A., Abdullatif, N., Faiz, R. "Modeling of CO_2 absorption in membrane contactors." *Separation and Purification Technology*. 59(3), pp. 286–293. 2008. https://doi.org/10.1016/j.seppur.2007.06.020

[2] Gabelman A., Hwang S-T. "Hollow fiber membrane contactors." *Journal of Membrane Science*. 159(1), pp. 61-106. 1999. https://doi.org/10.1016/S0376-7388(99)00040-X

[3] Qi, Z., Cussler, E. L. "Microporous hollow fibers for gas absorption Part 1: mass transfer in the liquid." *Journal of Membrane Science*. 23(3), pp. 321–332. 1985.

[4] Qi, Z., Cussler, E. L. "Microporous hollow fibers for gas absorption Part 2: mass transfer across the membrane." *Journal of Membrane Science*. 23(3), pp. 333–345. 1985. https://doi.org/10.1016/S0376-7388(00)83150-6

[5] Li, J. L., Chen, B. H. "Review of CO_2 absorption using chemical solvents in hollow fiber membrane contactors." *Separation and Purification Technology*. 41(2), pp. 109–122. 2005. https://doi.org/10.1016/j.seppur.2004.09.008

[6] Mansourizadeh, A., Ismail, A. F. "Hollow fiber gas-liquid membrane contactors for acid gas capture: a review" *Journal of Hazardous Materials*. 171(1-3), pp. 38-53. 2009. https://doi.org/10.1016/j.jhazmat.2009.06.026

[7] Zhang, H-Y., Wang, R., Liang, D. T., Tay J.-H. "Modeling and experimental study of CO_2 absorption in a hollow fiber membrane contactor." *Journal of Membrane Science.* 279(1-2), pp. 301–310. 2016. https://doi.org/10.1016/j.memsci.2005.12.017

[8] Sohrabi, M.R., Marjani, A., Moradi, S., Davallo, M., Shirazian, S. "Mathematical modeling and numerical simulation of CO_2 transport through hollow-fiber membranes." *Applied Mathematical Modelling.* 35(1), pp. 174–188. 2011. https://doi.org/10.1016/j.apm.2010.05.016

[9] Saidi, M., Heidarinejad, S., Rahimpour, H. R., Talaghat, M. R., Rahimpour, M. R. "Mathematical modeling of carbon dioxide removal using amine-promoted hot potassium carbonate in a hollow fiber membrane contactor." *Journal of Natural Gas Science and Engineering*. 18, pp. 274–285. 2014. https://doi.org/10.1016/j.jngse.2014.03.001

[10] Wang, R., Li, D.F., Liang, D. T. "Modeling of CO_2 capture by three typical amine solutions in hollow fiber membrane contactors." *Journal of Chemical Engineering & Process Technology.* 43(7), pp. 849–856. 2004. https://doi.org/10.1016/S0255-2701(03)00105-3

[11] Razavi, S. M. R., Razavi, S. M. J., Miri, T., Shirazian, S. "CFD simulation of CO_2 capture from gas mixtures in nanoporous membranes by solution of 2-amino-2-methyl-1-propanol and piperazine." *International Journal of Greenhouse Gas Control.* 15, pp. 142–149. 2013. https://doi.org/10.1016/j.ijggc.2013.02.011

[12] Bird, R. B., Stewart, W. E., Lightfoot, E. N. "*Transport Phenomena*." 2nd ed., John Wiley & Sons, New York. 2002.

[13] Versteeg, G. F., van Swaaij, W. P. M. "Solubility and diffusivity of acid gases (CO_2, N_2O) in aqueous alkanolamine solutions." *Journal of Chemical Engineering & Data*. 33(1), pp. 29-34. 1988. https://doi.org/10.1021/je00051a011

[14] Happel, J. "Viscous flow relative to arrays of cylinders." *AIChE Journal*. 5(2), pp. 174-177. 1959. https://doi.org/10.1002/aic.690050211

[15] Yang, M. C., Cussler, E. L. "Designing hollow-fiber contactors." *AIChE Journal*. 32(11), pp. 1910–1916. 1986. https://doi.org/10.1002/aic.690321117

[16] Crooks, J. E., Donnellan, J. P. "Kinetics and Mechanism of the Reaction between Carbon Dioxide and Amines in Aqueous Solution." *Journal of the Chemical Society, Perkin Transactions II*. 1(4), pp. 331-333. 1989. https://doi.org/10.1039/P29890000331

[17] Gilassi, S., Rahmanian, N. "CFD Modelling of a Hollow Fibre Membrane for CO_2 Removal by Aqueous Amine Solutions of MEA, DEA and MDEA." *International Journal of Chemical Reactor Engineering*. 14(1), pp. 53–61. 2016. https://doi.org/10.1515/ijcre-2014-0142

[18] Farjami, M., Moghadassi, A., Vatanpour, V. "Modeling and simulation of CO_2 removal in a polyvinylidene fluoride hollow fiber membrane contactor with computational fluid dynamics." *Chemical Engineering and Processing*. 98, pp. 41-51. 2015. https://doi.org/10.1016/j.cep.2015.10.006